Original Article

Construction and validation of a nomogram model for predicting peritoneal metastasis in gastric cancer based on ferroptosis-relate genes and clinicopathological features

Xiaotong Sun[1#], Kaipeng Duan[1#], Xiaochun Shen[2#], Chao Dong[1], Yajing Zhou[1], Tao Chen[1], Weikang Li[1], Peiyuan Li[1], Pengbo Wang[1], Dongbao Li[1], Jin Zhou[1]

[1]Department of General Surgery, The First Affiliated Hospital of Soochow University, Suzhou, China; [2]Department of Pulmonary and Critical Care Medicine, The First Affiliated Hospital of Soochow University, Suzhou, China

Contributions: (I) Conception and design: J Zhou, D Li, X Sun; (II) Administrative support: J Zhou, D Li; (III) Provision of study materials or patients: K Duan, X Shen, C Dong; (IV) Collection and assembly of data: X Sun, Y Zhou, T Chen, W Li; (V) Data analysis and interpretation: X Sun, P Li, P Wang; (VI) Manuscript writing: All authors; (VII) Final approval of manuscript: All authors.

[#]These authors contributed equally to this work.

Correspondence to: Jin Zhou, MD; Dongbao Li, MD. Department of General Surgery, The First Affiliated Hospital of Soochow University, 188 Shizi Street, Suzhou 215006, China. Email: zhoujinsuda@suda.edu.cn; ldbkap@163.com.

Background: Gastric cancer peritoneal metastasis (GCPM) is a lethal condition. Current diagnostic methods for GCPM, such as imaging and serum tumor markers, lack specificity and sensitivity. Research suggests that utilizing gene signatures to predict GCPM shows significant predictive ability. Nonetheless, the predictability of GCPM using ferroptosis-related genes (FRGs) remains unknown. We aim to construct a nomogram based on FRGs for early diagnosis of GCPM.

Methods: RNA sequencing and clinical data of patients with gastric cancer (GC) were downloaded from Gene Expression Omnibus (GEO) databases. GCPM was diagnosed through imaging, biopsy and cytology. A GCPM prediction model was developed based on six distinctively expressed FRGs, and the efficiency of the model was assessed through receiver operating characteristic (ROC) curves in both experimental and validation cohorts. Subsequently, 115 clinical samples were examined by immunohistochemistry (IHC) to validate the prediction model's accuracy.

Results: Our analysis included 282 patients, among whom 54 had GCPM while 228 did not. Patients were randomly distributed into experimental and validation groups at a 3:2 ratio. Least absolute shrinkage and selection operator (LASSO) regression identified the coefficients of six FRGs, with a risk score calculated for every patient. Univariate and multivariate logistic analyses revealed that both risk score and pathological stage were significantly associated with GCPM. The area under the curve (AUC) values for the training and validating sets implied good predictability for GCPM (0.827 and 0.767, respectively). Combining the risk score with the tumor node metastasis (TNM) stage substantially improved predictability (AUCs were 0.916 and 0.848 respectively). Lastly, a nomogram incorporating the risk score and TNM stage was constructed, which shows good clinical utility through decision curve analysis (DCA). The IHC results from 115 clinical samples were consistent with these findings.

Conclusions: A nomogram model based on FRGs and clinicopathological features was constructed, demonstrating impressive predictive value for GCPM. This enables timely and personalized therapeutic interventions, thereby benefiting gastric cancer patients.

Keywords: Gastric cancer (GC); peritoneal metastasis; ferroptosis; predictive signature; *RRM2*

Submitted Sep 03, 2024. Accepted for publication Jan 21, 2025. Published online Feb 26, 2025.
doi: 10.21037/jgo-24-670
View this article at: https://dx.doi.org/10.21037/jgo-24-670

Introduction

Gastric cancer (GC) is one of the most common gastrointestinal malignancies, ranking fifth in global cancer incidence and fourth in cancer-related mortality (1). Gastric cancer peritoneal metastasis (GCPM) refers to the spread of GC cells from the primary site to the peritoneum through various routes, including blood, lymph, or direct peritoneal growth. More than half of the patients with advanced GC develop peritoneal metastasis (PM) (2). Once PM is detected, the median overall survival (OS) is only 4–9 months (3). Approximately 60% of GC deaths are caused by GCPM (4). Occult peritoneal metastasis (OPM) refers to cases in which preoperative examinations, such as imaging, fail to detect PM, but postoperative pathology confirms its presence (2).

Chemotherapy is the standard treatment for patients with GCPM; however, the overall curative effect and prognosis after chemotherapy remain poor (5). Recent studies have demonstrated that systemic therapy or combination therapy of anti-angiogenesis therapy, immunotherapy and chemotherapy improves OS rates in patients with GC and PM (6-9). Recent randomized trials have demonstrated that cytoreductive surgery (CRS) combined with systemic immunotherapy, chemotherapy, and hyperthermic intraperitoneal chemotherapy (HIPEC) improves OS in patients with GCPM (10,11). Therefore, an accurate evaluation of the presence of PM is crucial for selecting an appropriate treatment method for patients with GC. Computed tomography (CT) is the most commonly used preoperative examination for diagnosing PM. However, occult peritoneal metastatic lesions are usually not visible on CT images. Although CT has high specificity, it lacks sensitivity for detecting PM (12). GCPM presents no specific symptoms in its early stages. Although imaging techniques such as CT, magnetic resonance imaging (MRI), and positron emission tomography (PET)-CT, along with blood tests including carcinoembryonic antigen (CEA), alpha fetoprotein (AFP), cancer antigen 125 (CA125), CA199, and CA72-4, improve the diagnostic rate, effective diagnosis remains a significant challenge. Laparoscopic and cytological examination of peritoneal lavage fluid is considered the gold standard for detecting OPM. However, these examinations are invasive and may be difficult for patients to accept. Therefore, there is an urgent need to develop new early diagnostic methods for GCPM.

Numerous studies have developed prediction models to forecast GCPM using various data sources, including imaging data, clinical characteristics, metabolomics, microRNA (miRNA), and long noncoding RNA (lncRNA). Dong combined CT scans with Lauren typing to construct a prediction model for GCPM, achieving an area under the curve (AUC) of 0.958 (2). Yang proposed a clinical nomogram by integrating clinical risk factors and radiomics features, achieving an AUC of 0.839 (13). Moreover, several studies have used ferroptosis-related genes (FRGs) to predict disease progression and prognosis. Xiong developed a risk model based on 10 ferroptosis regulators and markers and demonstrated a strong prognostic value for patients with ovarian cancer (14). Chen established a molecular signature based on 11 FRGs, which proved effective in assessing colorectal cancer prognosis (15). Our study highlights the elevated expression of cysteine protease inhibitor SN (Cystatin SN, *CST1*), which protects GC cells from ferroptosis, thereby promoting their progression and metastasis (16). Lin identified that the upregulation of hypoxia-inducible factor 1 alpha (*HIF-1α*) can shield GC cells from ferroptosis induced by the *HIF-1α/PMAN/*ELAVL1 pathway, suggesting it may be a potential driver of PM (17). In summary, this evidence emphasizes the need for innovative diagnostic and prognostic approaches focused on molecular and genetic markers associated with ferroptosis. Early intervention strategies can significantly improve survival outcomes in patients with GCPM.

Ferroptosis was first described by Dixon in 2012 (18). Ferroptosis is an iron-dependent form of regulated cell death that is caused by lipid peroxidation. This

Highlight box

Key findings

- A ferroptosis-related gene signature was constructed and demonstrated impressive predictive values for the peritoneal metastasis of gastric cancer (GCPM).

What is known and what is new?

- Currently effective early diagnostic methods for GCPM are lacking. Ferroptosis is highly correlated with GCPM.
- In this study, we constructed and verified an early diagnostic model for GCPM based on ferroptosis-related genes.

What is the implication, and what should change now?

- This study demonstrated that the six identified ferroptosis-related genes (*CDO1*, *AURKA*, *RRM2*, *CAV1*, *DDR2*, and *VLDLR*) are promising biomarkers for predicting the GCPM. The ferroptosis-associated gene signature depicts strong predictive efficiency for GCPM, offering a new avenue for exploring potential predictive biomarkers in this context.

process triggers immunosuppressive responses related to inflammation in the tumor microenvironment, thereby promoting tumor cell proliferation (19). Unlike apoptosis, necrosis, and autophagy, ferroptosis has unique genetic, morphological, and biochemical functions. The initial mechanism that triggers ferroptosis is the depletion of cysteine, which leads to the intracellular depletion of glutathione (GSH) (20). The activity of glutathione peroxidase 4 decreases, resulting in cellular lipid peroxidation and metabolic dysfunction. This leads to an increase in reactive oxygen species (ROS) levels, which in turn triggers ferroptosis. Previous studies have demonstrated that free iron concentration is higher in GC cells than in normal cells, and the survival of tumor cells is highly dependent on an abnormally activated antioxidant system (21-23). Further studies have demonstrated that the activation of ferroptosis can lead to GC cell death (24,25). Moreover, our findings indicate that the inhibition of ferroptosis accelerates GC metastasis (16). Many FRGs are closely related to the occurrence and development of GCPM and may affect the prognosis of patients with GC. Despite the strong correlation between ferroptosis and GCPM, there is currently no early diagnostic model for GCPM based on FRGs.

In this study, we analyzed the expression and predictive value of FRGs in predicting the occurrence of PM in patients with GC. Consequently, a six-FRG-based signature was constructed. Univariate and multivariate logistic analyses revealed that both FRGs-based signature and tumor node metastasis (TNM) pathological stage were significantly associated with GCPM. Receiver operating characteristic (ROC) curves were plotted to evaluate the predictive performance. The AUC values for the gene signature was 0.827 and 0.767 for the training and validation sets, respectively. For the TNM pathological stage, the AUC values were 0.785 and 0.716 in the training and validation sets, respectively. When the gene signature was combined with the TNM pathological stage, the predictive accuracy improved significantly, with AUC values of 0.916 and 0.848 in the training and validation sets, respectively. The model exhibited excellent predictive accuracy. To facilitate clinical application, a nomogram was constructed based on the 6-gene signature and TNM pathological stage to predict GCPM risk. Decision curve analysis (DCA) curves indicated that the nomogram was both reliable and accurate, potentially aiding clinicians in the early diagnosis of GCPM and planning personalized treatment strategies for patients with GC, thereby benefiting GC patients. Additionally, we performed immunohistochemistry (IHC) on 115 clinical samples to verify the expression of the six FRGs. In conclusion, we have successfully constructed an early diagnostic model for GCPM based on FRGs. We present this article in accordance with the TRIPOD reporting checklist (available at https://jgo.amegroups.com/article/view/10.21037/jgo-24-670/rc).

Methods

Data source

The study process is illustrated in *Figure 1*. The messenger RNA (mRNA) transcriptome data and corresponding clinical data from 300 GC samples, both with and without PM, were obtained from the Gene Expression Omnibus (GEO) database (https://www.ncbi.nlm.nih.gov/geo), specifically from the GSE62254 dataset (procured n=300 primary independent GC specimens at the time of total or subtotal gastrectomy at Samsung Medical Centre, Seoul, Korea, from 2004–2007). No subjects received neoadjuvant chemotherapy or chemoradiation therapy. Cases were selected on the basis of the following criteria: histologically confirmed adenocarcinoma of the stomach; surgical resection of primary GC; age ≥18 years; and complete pathological, surgical, treatment, and follow-up data. Two expert gastrointestinal pathologists (Kyoung-Mee Kim, MD; In-Gu Do, MD) reviewed hematoxylin and eosin (H&E)-stained slides to select cases with estimated carcinoma content of at least 60%. They clinically annotated the tumors but de-linked them from personally identifiable information. This cohort has a median follow-up time of 86.4 months (range, 53.1–106.6 months). The post-operative surveillance program for recurrence is to follow up every 6 months until 5 years from the date of surgery. They used OS as the primary endpoint. OS is defined as the time from surgery to the date of death or to the last follow-up date. They defined the date of relapse as the date of documented recurrences by imaging, biopsy and cytology. They used the date of last follow up for cases with no recurrence at the time of the last follow up. They retrospectively reviewed the pattern of recurrence, all CT imaging and medical records). After excluding 18 cases with incomplete data, 54 of the remaining 282 samples had PM, whereas 228 did not. The samples were randomly divided into experimental (n=168) and validation (n=114) groups in a 3:2 ratio for further analysis. The FRGs were obtained from the FerrDB (http://www.zhounan.org/ferrdb). Primary GC tissues and

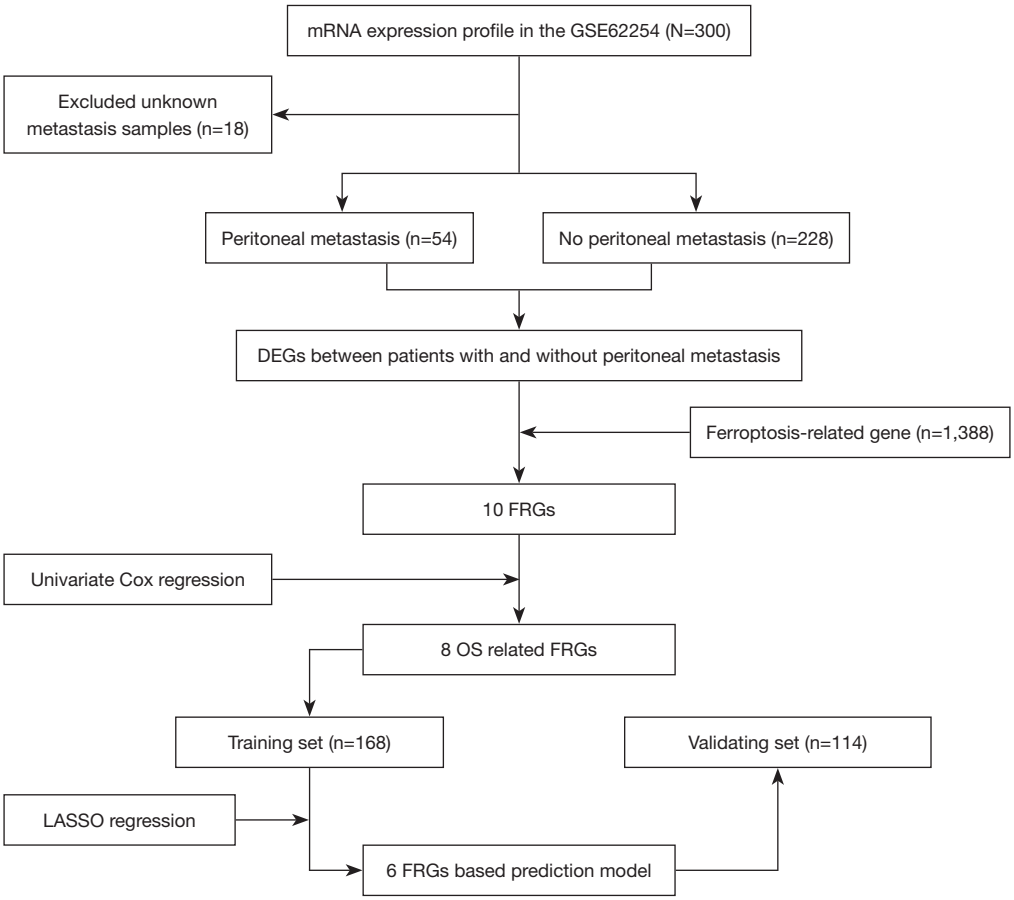

Figure 1 Flowchart showing the process of constructing the FRGs based signature to predict the possibility of peritoneal metastasis in gastric cancer. DEGs, differently expressed genes; FRGs, ferroptosis-related genes; OS, overall survival; LASSO, least absolute shrinkage and selection operator.

corresponding clinical data were collected from 115 patients with and without GCPM who underwent gastric resection for GC without neoadjuvant therapy at the First Affiliated Hospital of Soochow University between 2010 and 2020. All the patients underwent surgical treatment at the First Affiliated Hospital of Soochow University and there were none previous chemotherapies, radiotherapies, or other treatments before surgery on these patients. The diagnosis of GCPM is based on pathological findings.

Identification of FRGs

We utilized the "limma" package to screen for differentially expressed genes (DEGs) in the GSE62254 dataset related to GCPM. The threshold for identifying DEGs was set at $|\log_2 FC| > 1$ and $P<0.05$. Overlapping genes between the DEGs from the GSE62254 dataset and FRGs were selected.

Construction of an FRG signature

Univariate Cox regression analysis was used to identify the survival-related FRGs. The coefficients of these survival-related FRGs were then analyzed using least absolute shrinkage and selection operator (LASSO) regularized linear Cox regression. The risk score for each patient was calculated using the following formula: risk score = $h0(t) * \exp(\beta 1X1 + \beta 2X2 + \ldots + \beta nXn)$. Therefore, an FRG-based signature was obtained. This formula was used to derive the FRG-based signature. Patients were categorized into high- and low-risk groups based on the median risk score cutoff.

Correlation analysis between the FRGs signature and clinical characteristics

Clinical information, including age, gender, TNM stage,

Lauren classification, and survival information, was collected from the GC data in the GSE62254 dataset. Univariate and multivariate logistic regression analyses revealed that both risk score and TNM stage were significantly associated with PM. A nomogram combining the six-FRG signature and the TNM stage was constructed to predict the risk of GCPM. ROC and Kaplan-Meier (KM) curves were plotted to evaluate the prediction accuracy and prognostic value in both the training and validation sets. DCA curves were used to assess the clinical effectiveness of the model.

Functional enrichment analysis

Gene Ontology (GO) and Kyoto Encyclopedia of Genes and Genomes (KEGG) pathway analyses were performed using The Database for Annotation, Visualization and Integrated Discovery (DAVID) database (https://david.ncifcrf.gov) with standard settings. GO terms and KEGG pathways were ranked by P [or $-\log_{10}(P)$] using a cutoff of <0.05. Metascape (https://metascape.org/gp/index.html#/main/step1) was used for complementary annotation.

IHC validation of FRG expression in clinical samples

The expression levels of the six FRGs were validated in clinical samples by IHC. Primary GC samples and clinical information were collected from 115 patients with and without GCPM who underwent gastric resection without neoadjuvant therapy at the First Affiliated Hospital of Soochow University between 2010 and 2020. Samples were either stored at –80 ℃ or fixed in 10% formalin and embedded in paraffin for IHC. Five-micron-thick paraffin-embedded sections were used for IHC staining. The IHC sections were scanned with NanoZoomer S60 (Hamamatsu Photonics) and analyzed using ImageJ software. The final expression score was determined based on the median value: scores below the median indicated low expression, whereas scores above the median indicated high expression.

Written informed consent was obtained from all patients. This study was conducted in accordance with the principles of the Declaration of Helsinki (as revised in 2013) and approved by the Ethics Committee of the First Affiliated Hospital of Soochow University (approval No. 2020381).

Statistical analyses

The Chi-squared and Fisher's exact tests were used to compare differences between the training and validation sets, as well as between patients with GC with and without PM. Univariate Cox regression, univariate logistic regression, multivariate logistic regression, and LASSO logistic regression analyses were performed using R. DCA was performed to evaluate the clinical utility of the predictive models. KM survival curves were generated to illustrate the relationship between the risk score and OS, and significance was tested using the log-rank test. ROC curves were plotted to assess the prognostic accuracy. AUC was used to define predictive ability, with AUC >0.7 considered acceptably predictive. *T*-tests were used for statistical analyses in IHC. All statistical tests were two-sided, with a P<0.05 was considered statistically significant. Statistical analyses were conducted using the Statistical Package for Social Sciences (SPSS) software (version 28.0.0; SPSS Inc., Chicago, IL, USA) or R (version 4.2.2).

Results

Screening of FRGs associated with GCPM

mRNA transcriptomic data, along with the corresponding clinicopathological and survival information, were obtained for 300 GC tumor tissues from the GSE62254 cohort. The principal component analysis (PCA) plot is displayed in *Figure 2A*, and normalization of the mRNA transcriptomic data is presented in *Figure 2B*. After excluding 18 cases with incomplete data, 54 of the remaining 282 samples had PM, whereas 228 did not. These samples were randomly divided into training (n=168) and validation (n=114) groups in a 3:2 ratio. Non-significant differences were found between the two groups in terms of sex, age, pathological stage, Lauren classification, and lymph node metastasis (*Table 1*). A total of 390 DEGs ($|\log FC| > 1$, P<0.05) associated with GCPM were identified. These DEGs intersected with 934 known FRGs from the Ferroptosis Database (FerrDB), resulting in ten differentially expressed FRGs associated with PM in GC (*Figure 2C*). Finally, LASSO regression confirmed that six FRGs were significantly associated with GCPM, and their coefficients were used to calculate the risk score for GCPM (*Figure 2D-2F*), which was based on eight prognostic FRGs identified by univariate and multivariate Cox regression analyses (*Figure 3*). The six FRGs are cysteine dioxygenase 1 (*CDO1*), aurora kinase A (*AURKA*), ribonucleotide reductase subunit M2 (*RRM2*), caveolin-1 (*CAV1*), discoidin domain receptor 2 (*DDR2*), and very-low-density lipoprotein receptor (*VLDLR*).

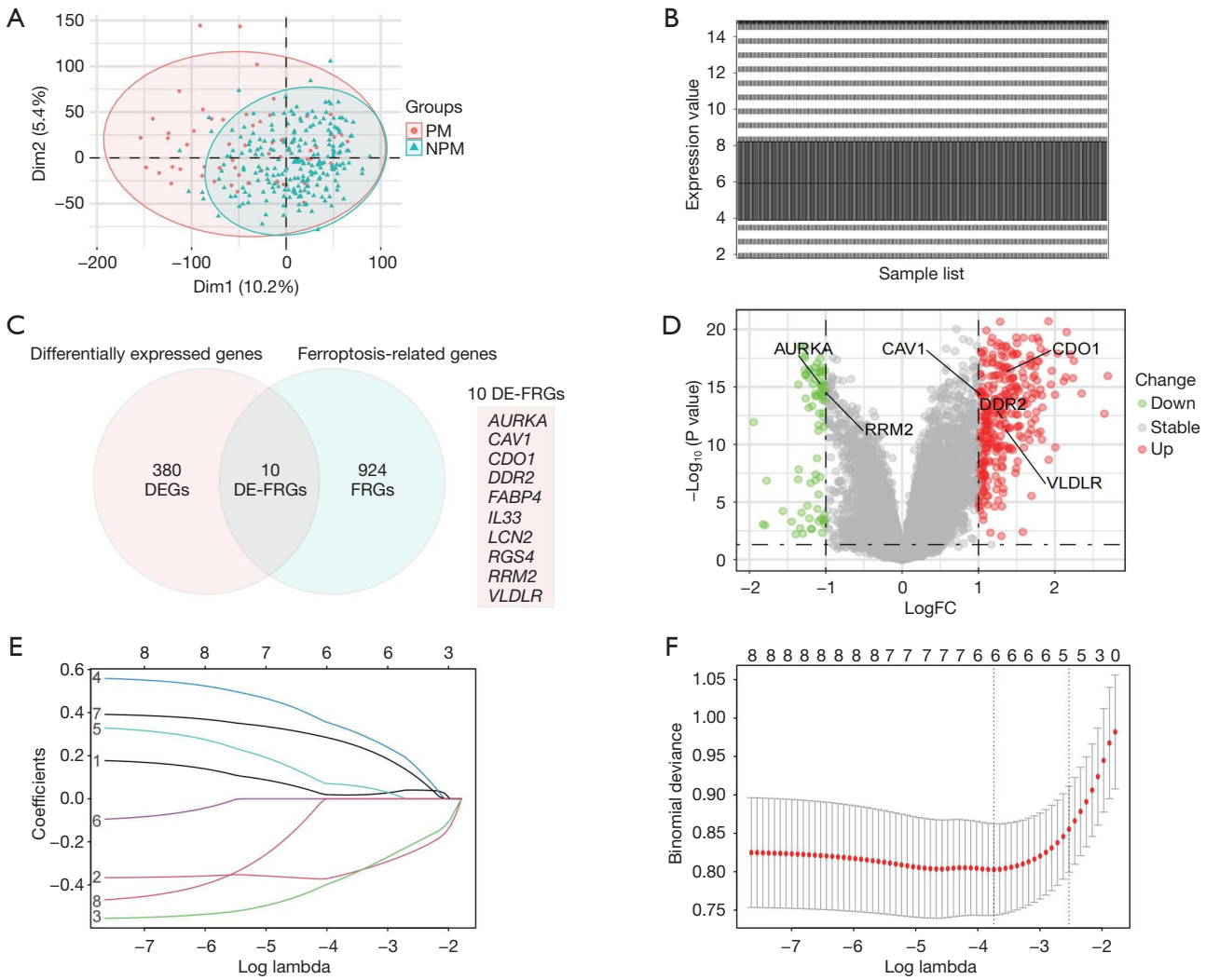

Figure 2 Construction of a FRGs signature. (A) PCA of the transcriptome profiles of two groups. (B) GSE62254 datasets after standardization. (C) The Venn plot shows the differently expressed FRGs associated with GCPM. (D) The volcano plot shows the differently expressed genes between PM and NPM. (E) LASSO regression of 10 FRGs genes. (F) Cross validation of parameter selection in LASSO regression. PCA, principal component analysis; FRGs, ferroptosis-related genes; GCPM, gastric cancer peritoneal metastasis; PM, peritoneal metastasis; NPM, no peritoneal metastasis; LASSO, least absolute shrinkage and selection operator; DE-FRGs, differently expressed ferroptosis-related genes.

Construction and validation of a prediction model based on six FRGs for predicting peritoneal metastasis in GC

Heatmaps of both the training and validation groups indicated that high expression levels of *CDO1*, *CAV1*, *DDR2*, and *VLDLR* were associated with an increased risk of GCPM, whereas high expression levels of *AURKA* and *RRM2* were associated with a decreased risk of GCPM (*Figure 4A*,*4B*). The risk score for each patient was calculated using the coefficients derived from the LASSO regression model with the following formula: risk score = (0.01774626 × expression value of *CDO1*) − (0.35365977 × expression value of *AURKA*) − (0.36934131 × expression value of *RRM2*) + (0.33121864 × expression value of *CAV1*) + (0.06607238 × expression value of *DDR2*) + (0.26560915 × expression value of *VLDLR*). The patients were categorized into high- and low-risk groups based on the median risk score. KM survival curves demonstrated that OS was significantly shorter for the high-risk group compared to

the low-risk group, both in the training (P=0.01, *Figure 4C*) and validation (P=0.002, *Figure 4D*) sets. Similarly, disease-free survival analyses depicted significant differences between the high-risk and low-risk groups in both the training (P=0.03, *Figure 4E*) and validation sets (P=0.005, *Figure 4F*).

Table 1 Clinical features of public databases gastric cancer patients

Characteristics	Training set (n=168)	Testing set (n=114)	P
Sex			>0.99
F	57 (33.9)	39 (34.2)	
M	111 (66.1)	75 (65.8)	
Age (years)			>0.99
≤65	98 (58.3)	66 (57.9)	
>65	70 (41.7)	48 (42.1)	
Lauren's classification			0.33
Diffuse & mixed	81 (48.2)	62 (54.4)	
Intestinal	87 (51.8)	52 (45.6)	
Lymph node metastasis			>0.99
Negative	20 (11.9)	14 (12.3)	
Positive	148 (88.1)	100 (87.7)	
pStage			0.14
I & II	75 (44.6)	40 (35.1)	
III & IV	93 (55.4)	74 (64.9)	

Data are presented as n (%). F, female; M, male; pStage, pathological stage.

Enhancing prediction accuracy by combining the gene signature with clinical characteristics

Univariate and multivariate logistic analyses revealed that both risk score and TNM pathological stage were significantly associated with GCPM. ROC curves were plotted for both the training and validation sets to evaluate the predictive performance of the gene signature and the TNM pathological stage. AUC for the gene signature was 0.827 and 0.767 for the training and validation sets, respectively. For the TNM pathological stage, the AUC values were 0.785 and 0.716 in the training and validation sets, respectively. When the gene prediction model was combined with the TNM pathological stage, the predictive accuracy improved significantly, with AUC values of 0.916 and 0.848 in the training and validation sets, respectively (*Figure 4G*,*4H*). The forest plots for univariate and multivariate logistic regression analyses are presented at *Figures 5*,*6*. To facilitate clinical application, a nomogram was constructed based on the 6-gene signature and TNM pathological stage to predict GCPM risk (*Figure 7A*). DCA curves indicated that the nomogram was both reliable and accurate (*Figure 7B*,*7C*), potentially aiding clinicians in the early diagnosis of GCPM and planning personalized

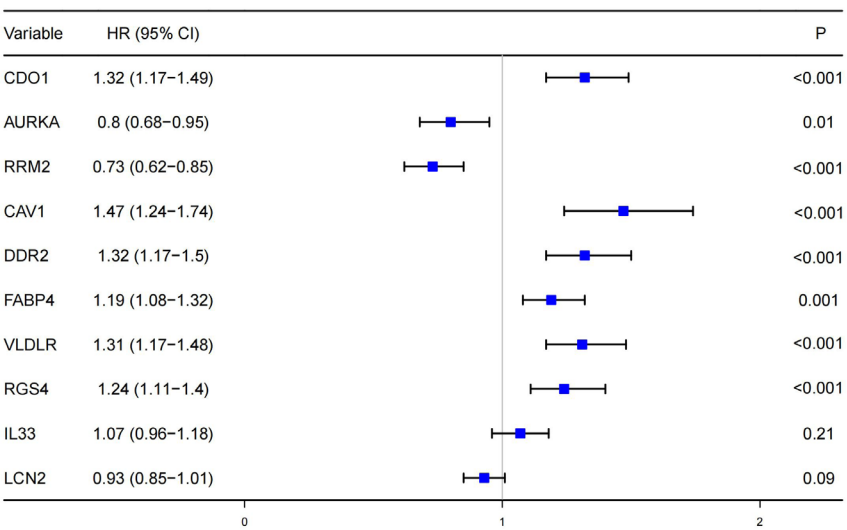

Figure 3 Univariate Cox analysis of the 10 FRGs with OS. HR, hazard ratio; CI, confidence interval; FRGs, ferroptosis-related genes; OS, overall survival.

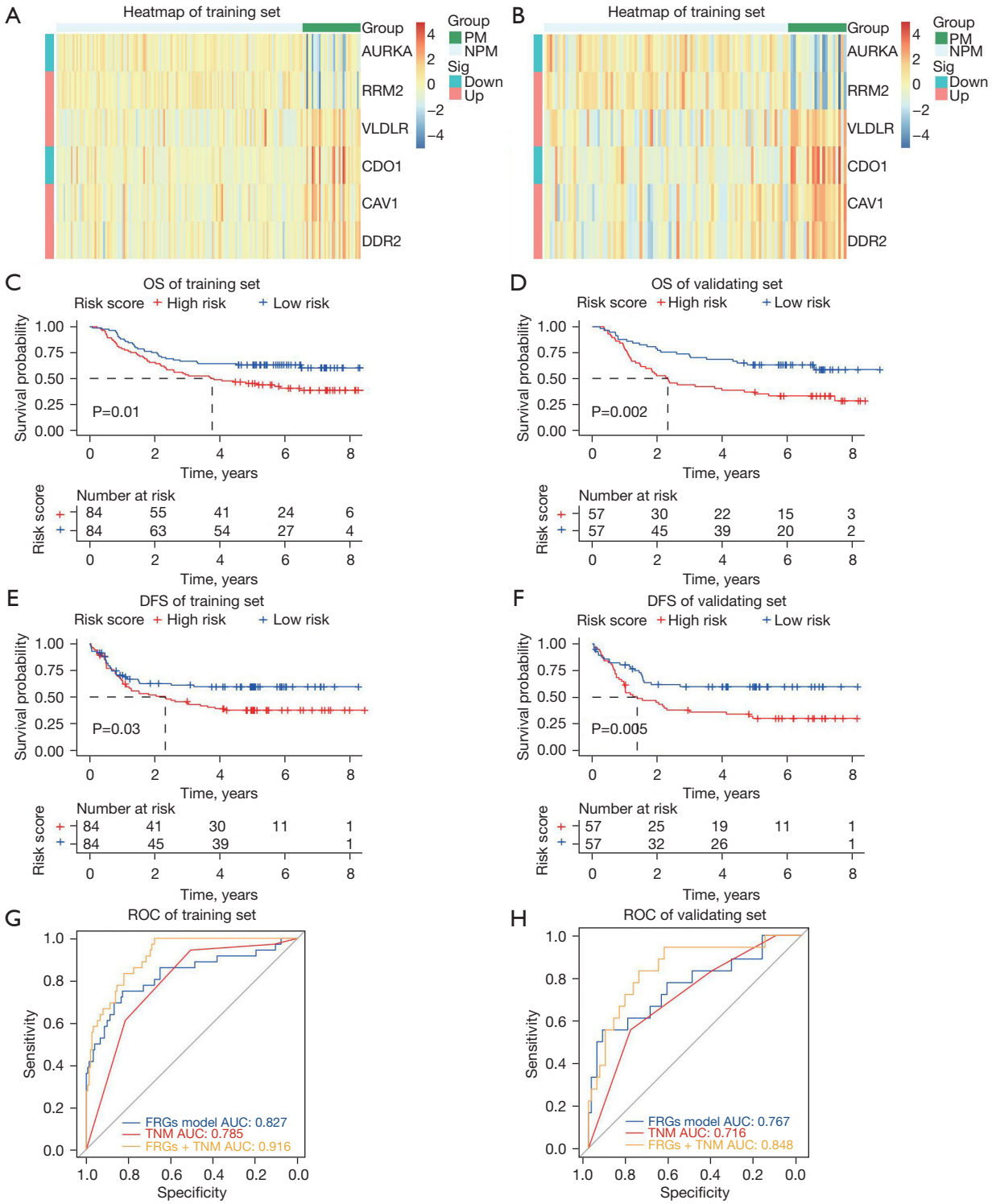

Figure 4 Validation of the 6 FRGs-based signature in the training set and the validating set. (A,B) The heatmap of the 6 FRGs expression profiles. (C,D) KM analysis for OS of GC patients based on the risk stratification. (E,F) KM analysis for DFS of GC patients based on the risk stratification. (G,H) ROC analysis for the risk of PM including the risk score, TNM stage and combination of the two. PM, peritoneal metastasis; NPM, no peritoneal metastasis; OS, overall survival; DFS, disease-free survival; ROC, receiver operating characteristic curve; FRGs, ferroptosis-related genes; AUC, areas under the curve; TNM, tumor node metastasis; KM, Kaplan-Meier; GC, gastric cancer.

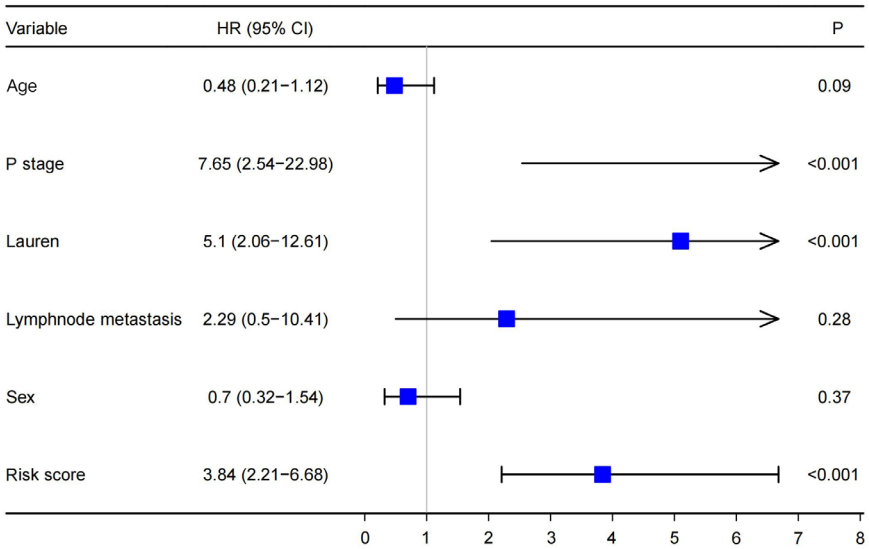

Figure 5 Univariate logistics analysis of the 6 FRGs-based signature with peritoneal metastasis. HR, hazard ratio; CI, confidence interval; pStage, pathological stage; FRGs, ferroptosis-related genes.

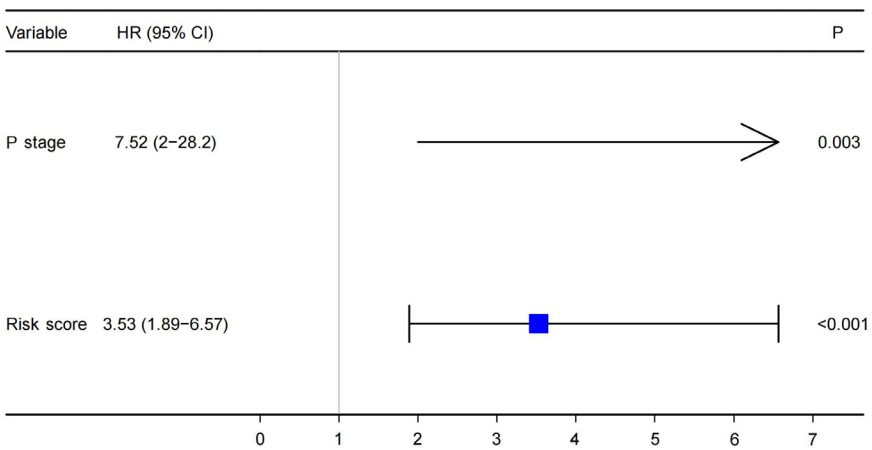

Figure 6 Multivariate logistics analysis of the 6 FRGs-based signature with peritoneal metastasis. HR, hazard ratio; CI, confidence interval; pStage, pathological stage; FRGs, ferroptosis-related genes.

treatment strategies for patients with GC.

Pathway enrichment analysis

Functional enrichment analysis was performed using DAVID and Metascape tools, revealing several significant insights. GO analysis identified that the top 100 related genes were primarily enriched in biological processes such as mitotic nuclear division and extracellular matrix organization. In cellular components, these genes were mainly associated with condensed chromosomes, centromeric regions, and collagen-containing extracellular matrix. Molecular functions analysis depicted that the genes were generally enriched in integrin binding and actin binding (*Figure 8A*).

KEGG pathway analysis revealed that these genes were significantly enriched in several pathways, including epithelial cell signaling in *Helicobacter pylori* infection, cell adhesion molecules, cell cycle, extracellular matrix (ECM)-receptor interaction, p53 signaling pathway, and interleukin 17 (IL-17) signaling pathway (*Figure 8B*). Additionally, Metascape analysis indicated significant enrichment in

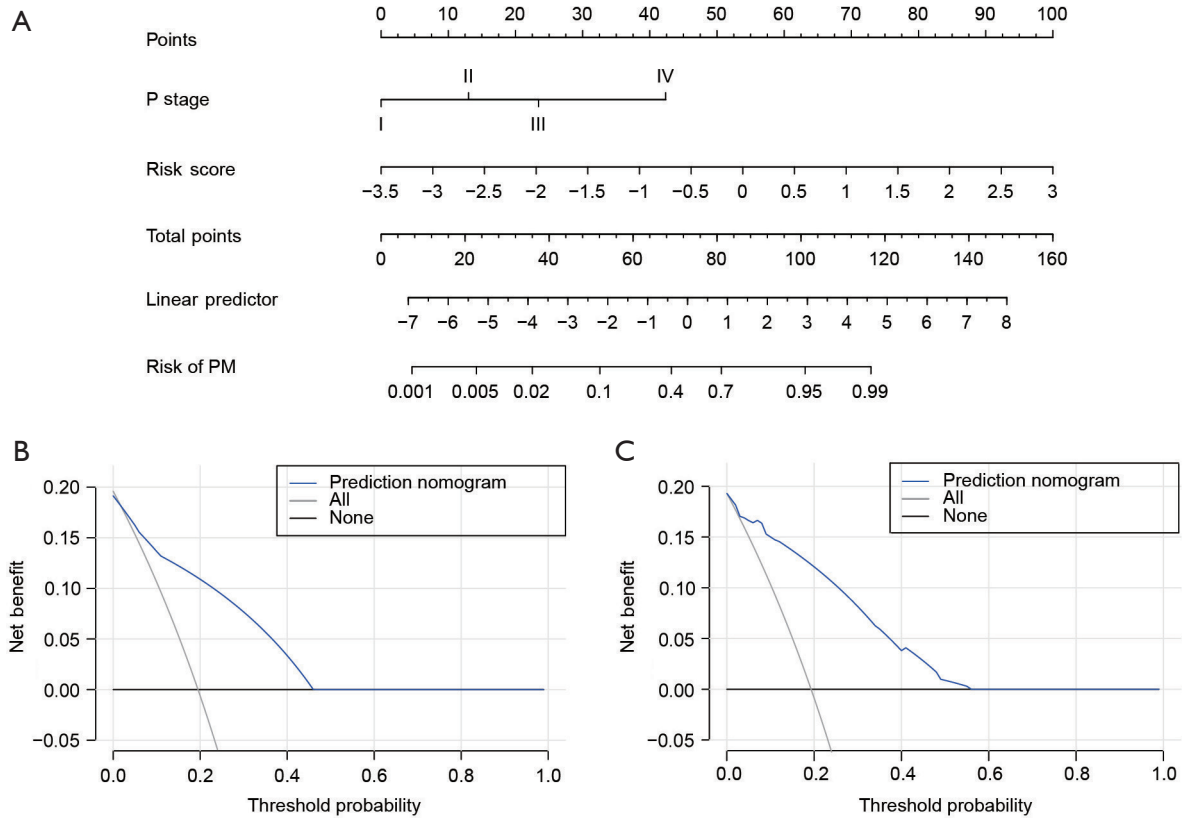

Figure 7 Nomogram to predict the risk of GCPM. (A) Nomogram to predict the risk of GCPM. (B) DCA of the nomogram in training set. (C) DCA of the nomogram in validation set. pStage, pathological stage; PM, peritoneal metastasis; GCPM, gastric cancer peritoneal metastasis; DCA, decision curve analysis.

processes such as cellular anatomical entity morphogenesis, cell growth and cell-substrate regulation, cell-cell adhesion, positive regulation of epithelial cell proliferation, and regulation of actin filament-based processes (*Figure 8C*,*8D*). These findings suggest that the identified pathways are closely associated with PM of GC.

IHC validated the expression levels of six FRGs in clinical samples

To validate the expression levels of the six identified FRGs (*CDO1*, *CAV1*, *DDR2*, *VLDLR*, *AURKA*, and *RRM2*), IHC analysis was performed on 115 clinical samples from patients with GC. This cohort included 22 patients with PM and 93 patients without PM. The clinical characteristics of patients are presented in *Table 2*. Our analysis revealed that *CDO1*, *CAV1*, *DDR2*, and *VLDLR* were overexpressed in patients with PM compared to those without PM, while *AURKA* and *RRM2* were overexpressed in patients without PM compared to those with GCPM (*Figure 9A-9F*). These IHC results align with the bioinformatics analysis previously discussed, thereby reinforcing the credibility of bioinformatic predictions.

Discussion

More than half of GC-related deaths are attributed to GCPM (5). GCPM presents no specific symptoms in its early stages. Although imaging techniques such as CT, MRI, and PET-CT, along with blood tests including CEA, AFP, CA125, CA199, and CA72-4, improve the diagnostic rate, effective diagnosis remains a significant challenge. In many cases, PM in patients with advanced GC is identified only during or shortly after radical surgery. Even after patients undergo radical resection, the disease often progresses, resulting in a poor prognosis. The prognosis of patients with GC and PM can be significantly improved through neoadjuvant therapy, systemic chemotherapy,

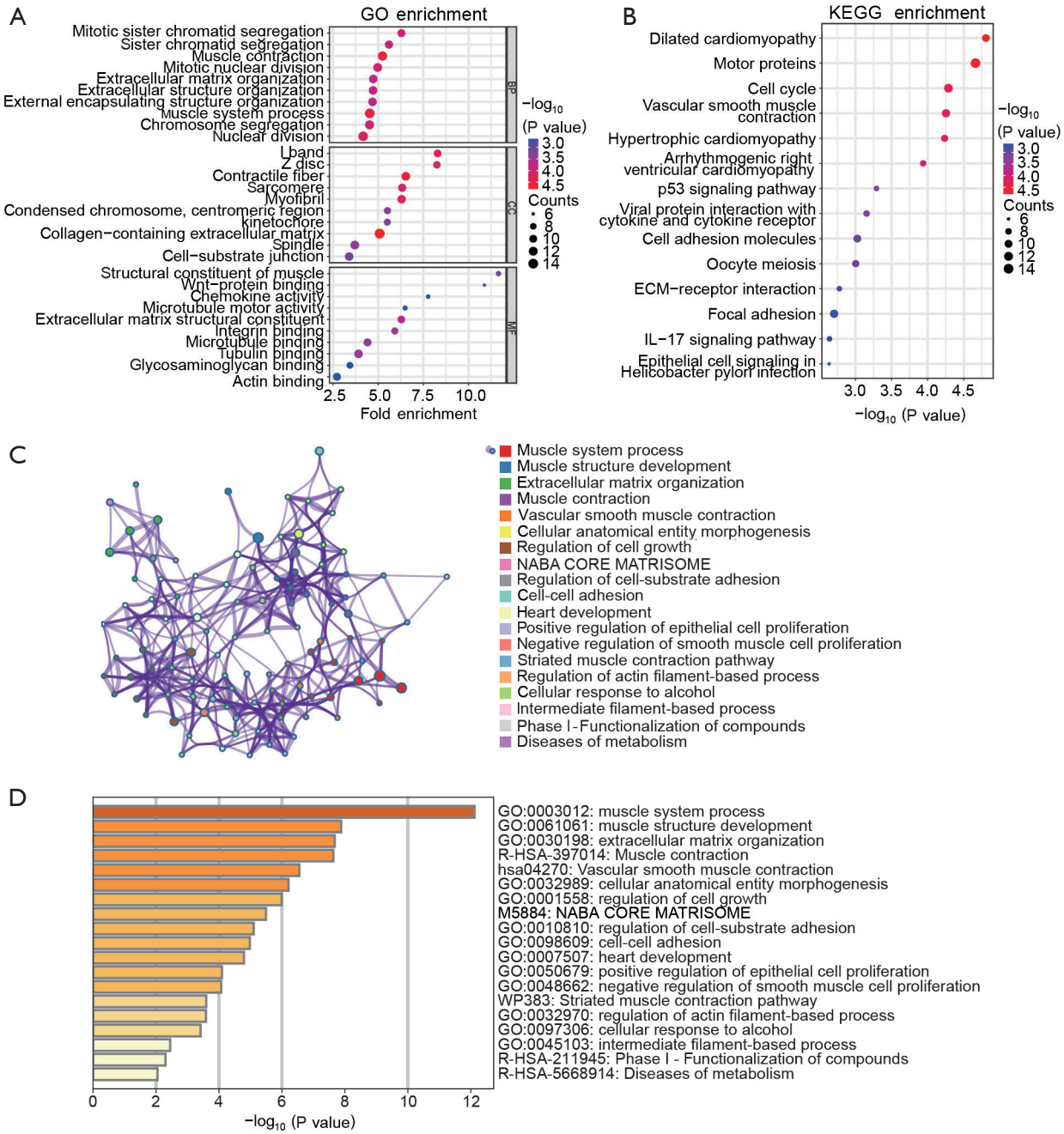

Figure 8 Pathway enrichment analysis of the related DEGs. (A) Dotplot of GO enrichment analysis. (B) Dotplot of KEGG enrichment analysis. (C,D) Pathways enriched by Metascape. GO, Gene Ontology; KEGG, Kyoto Encyclopedia of Genes and Genomes; ECM, extracellular matrix; IL, interleukin; BP, biological process; CC, cellular component; MF, molecular function; DEGs, differently expressed genes.

immunochemotherapy, CRS, and HIPEC. Screening high-risk cases of PM through preoperative examinations and developing tracer methods for intraoperative diagnosis can enhance OPM detection, leading to better treatment outcomes. There is an urgent need for a high-performance method for early diagnosis of GCPM to facilitate the

Table 2 Clinical features of clinical gastric cancer patients

Characteristics	Overall (n=115)
Sex	
F	34 (29.6)
M	81 (70.4)
Age (years)	
≤65	52 (45.2)
>65	63 (54.8)
Peritoneal metastases	
Negative	93 (80.9)
Positive	22 (19.1)
pStage	
I	4 (3.5)
II	37 (32.2)
III	25 (21.7)
IV	49 (42.6)

Data are presented as n (%). F, female; M, male; pStage, pathological stage.

development of appropriate treatment plans and timely intervention.

Numerous studies have developed prediction models to forecast GCPM using various data sources, including imaging data, clinical characteristics, metabolomics, miRNA, and lncRNA. Dong combined CT scans with Lauren typing to construct a prediction model for GCPM, achieving an AUC of 0.958 (2). Yang proposed a clinical nomogram by integrating clinical risk factors and radiomics features, achieving an AUC of 0.839 (13). Moreover, several studies have used FRGs to predict disease progression and prognosis. Xiong developed a risk model based on 10 ferroptosis regulators and markers and demonstrated a strong prognostic value for patients with ovarian cancer (14). Chen established a molecular signature based on 11 FRGs, which proved effective in assessing colorectal cancer prognosis (15). Our study highlights the elevated expression of cysteine protease inhibitor SN (Cystatin SN, *CST1*), which protects GC cells from ferroptosis, thereby promoting their progression and metastasis (16). Lin identified that the upregulation of *HIF-1α* can shield GC cells from ferroptosis induced by the *HIF-1α*/*PMAN*/ELAVL1 pathway, suggesting it may be a potential driver of PM (17). In summary, this evidence emphasizes the need for innovative diagnostic and prognostic approaches focused on molecular and genetic markers associated with ferroptosis. Early intervention strategies can significantly improve survival outcomes in patients with GCPM.

FRGs play a critical role in GCPM and may serve as key targets for both diagnosis and treatment. This study developed a prediction model based on six FRGs to assess the GCPM risk. The model exhibited excellent predictive accuracy, and when combined with TNM staging, its ability to predict GCPM significantly improved, with AUC values of 0.916 and 0.848 in the training and validation sets, respectively. To support its clinical use, we constructed nomogram plots featuring two parameters: risk score and TNM stage. The DCA curve demonstrated a strong clinical applicability. Notably, high expression of *CDO1*, *CAV1*, *DDR2*, and *VLDLR* was associated with an increased risk of GCPM, whereas high expression of *AURKA* and *RRM2* was associated with a decreased risk.

Human *CDO1* is a non-heme iron dioxygenase that catalyzes the oxidation of cysteine-to-cysteine sulfinic acid (26). Cellular cysteine is an essential substrate for GSH synthesis (27). A reduction in GSH synthesis increases ROS levels, which can lead to ferroptosis (28-30). Ushiku *et al.* identified that *CDO1* gene promoter DNA methylation, detectable through quantitative methylation-specific PCR, holds significant potential for detecting minimal residual disease in the peritoneum within clinical settings for GC (31). *AURKA* regulates centrosome functions and is essential for mitotic progression (32). Overexpression of *AURKA* leads to centrosome amplification and cytokinetic failure, causing aneuploidy (33). *AURKA* is also involved in regulating several key proteins in cancer cells, such as AKT, β-catenin, and p53, which may contribute to cancer development (34-38). Furthermore, *AURKA* regulates histone modification through the Wnt/β-catenin and PI3K/Akt signaling pathways to induce epithelial-mesenchymal transition (EMT) in GC (39). *AURKA* may also play a role in regulating ferroptosis, with its overexpression potentially protecting cancer cells from ferroptosis (40-42). *RRM2* is a small regulatory subunit of ribonucleotide reductase that is essential for deoxynucleoside triphosphate (dNTP) biogenesis (43). Regulation of dNTP levels is crucial for DNA replication and cell proliferation (44). *RRM2* inhibition can enhance chemosensitivity and overcome drug resistance in fibrosarcoma and pancreatic cancer (45,46). *RRM2* is highly expressed in GC cells (BGC823), and the *RRM2*/AKT/NF-κB signaling pathway plays a critical role in promoting tumor invasiveness (47). *CAV1* functions as a membrane adaptor that links the integrin alpha subunit

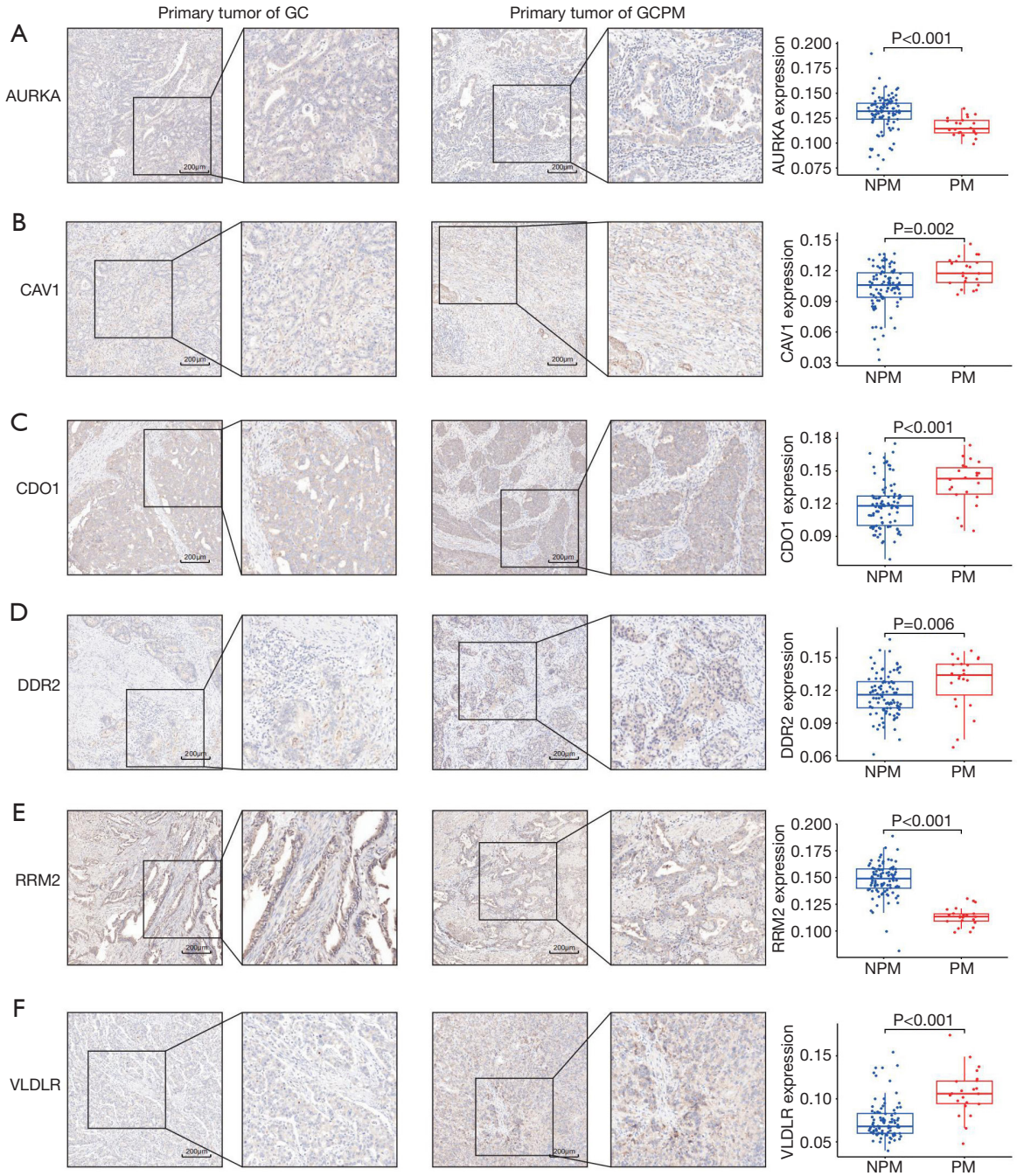

Figure 9 Validation of the 6 FRGs in clinical samples. (A-F) IHC staining and expression of the 6 FRGs in primary GC lesions. Left-side images: 100× magnification; right-side images: 200× magnification. GC, gastric cancer; GCPM, gastric cancer peritoneal metastasis; NPM, no peritoneal metastasis; PM, peritoneal metastasis; FRGs, ferroptosis-related genes; IHC, immunohistochemistry.

to tyrosine kinases and plays an essential role in integrin signaling, endocytosis, and anchorage-dependent cell growth (48,49). High *CAV1* expression is associated with poor prognosis in patients with GC (50,51). Furthermore, *CAV1* promotes chemoresistance to cisplatin in GC cells by activating the WNT/β-Catenin pathway (52). *DDR2*, a receptor tyrosine kinase, is activated by binding to both fibrillar and non-fibrillar collagen (53,54). *DDR2* promotes

tumor formation and invasion by enhancing EMT through mTORC2 activation and AKT phosphorylation (55). It also contributes to maintaining GC stemness and DNA damage repair in cancer stem cells and promotes tumor peritoneal dissemination, as observed in a gastric xenograft mouse model (56). V*LDLR* is involved in the uptake of low-density lipoprotein (LDL) and very-low-density lipoprotein and belongs to the LDL receptor superfamily (57). *VLDLR* is highly expressed in various tumors, including in the stomach, breasts, and lungs (58-60). *VLDLR* influences numerous cellular functions owing to its ability to bind a range of ligands, including lipoprotein lipase (61), receptor-associated protein (62) and thrombospondin-1 (63).

This study demonstrated that the six identified FRGs (*CDO1*, *AURKA*, *RRM2*, *CAV1*, *DDR2*, and *VLDLR*) are promising biomarkers for predicting PM in GC. The gene signature linked to ferroptosis demonstrated strong predictive efficiency for GCPM, offering a new path for identifying potential biomarkers in this context. However, there are some limitations in this study. Including the constraints of the GEO database, such as limited sample size, potential batch effects, and heterogeneity in data collection and processing, which may impact the robustness and generalizability of the predictive value of these gene signatures. Clinical data from large multicenter samples are crucial to validate the predictive accuracy of these findings. Further research and validation through larger clinical trials are needed to fully integrate these biomarkers into standard clinical practice to benefit patients with GC.

Conclusions

We developed a novel nomogram model based on FRGs to predict GCPM by integrating the DEGs associated with GCPM and FRGs. This model, which includes six FRGs (*CDO1*, *AURKA*, *RRM2*, *CAV1*, *DDR2*, and *VLDLR*), was validated through multiple approaches and demonstrated a robust predictive value for patients with GC who developed GCPM. The prediction model utilizing these six FRGs demonstrates high practicality for clinical application, aiding in early diagnosis and potentially improving GCPM management. This nomogram could significantly help identify patients at high risk for PM, thereby enabling timely and personalized therapeutic interventions.

Acknowledgments

None.

Footnote

Reporting Checklist: The authors have completed the TRIPOD reporting checklist. Available at https://jgo.amegroups.com/article/view/10.21037/jgo-24-670/rc

Data Sharing Statement: Available at https://jgo.amegroups.com/article/view/10.21037/jgo-24-670/dss

Peer Review File: Available at https://jgo.amegroups.com/article/view/10.21037/jgo-24-670/prf

Funding: This work was supported by the National Natural Science Foundation of China (NSFC, grant Nos. 81871952, 82372887, 82403045), the Natural Science Foundation of Jiangsu Province (grant Nos. BK20221242, BK20240372), Gusu Health Talents Cultivation Program, China (grant No. GSWS2019008), the "Qinglan Project" in Jiangsu Colleges and Universities, the Special Project of Diagnosis and Treatment Technology for Clinical Key Diseases in Suzhou (grant No. LCZX202202), the Clinical Medicine Peak Project of Suzhou Medical College of Soochow University, the Leading Talent Project of "Boxi Excellent Talent Training Plan" of the First Affiliated Hospital of Soochow University, the Youth Science and Technology of Suzhou Science and Education Project (grant No. KJXW2023005), Boxi Youth Natural Science Foundation of the First Affiliated Hospital of Soochow University (grant No. BXQN2023027).

Conflicts of Interest: All authors have completed the ICMJE uniform disclosure form (available at https://jgo.amegroups.com/article/view/10.21037/jgo-24-670/coif). The authors have no conflicts of interest to declare.

Ethical Statement: The authors are accountable for all aspects of the work in ensuring that questions related to the accuracy or integrity of any part of the work are appropriately investigated and resolved. This study was conducted in accordance with the principles of the Declaration of Helsinki (as revised in 2013) and approved by the Ethics Committee of the First Affiliated Hospital of Soochow University (approval No. 2020381). Written informed consent was obtained from all patients.

References

1. Bray F, Laversanne M, Sung H, et al. Global cancer statistics 2022: GLOBOCAN estimates of incidence and mortality worldwide for 36 cancers in 185 countries. CA Cancer J Clin 2024;74:229-63.
2. Dong D, Tang L, Li ZY, et al. Development and validation of an individualized nomogram to identify occult peritoneal metastasis in patients with advanced gastric cancer. Ann Oncol 2019;30:431-8.
3. Rijken A, Pape M, Simkens GA, et al. Peritoneal metastases from gastric cancer in a nationwide cohort: Incidence, treatment and survival. Int J Cancer 2024;154:992-1002.
4. Tiwari A, Swamynathan S, Jhanji V, et al. KLF4 Coordinates Corneal Epithelial Apical-Basal Polarity and Plane of Cell Division and Is Downregulated in Ocular Surface Squamous Neoplasia. Invest Ophthalmol Vis Sci 2020;61:15.
5. Ajani JA, D'Amico TA, Bentrem DJ, et al. Gastric Cancer, Version 2.2022, NCCN Clinical Practice Guidelines in Oncology. J Natl Compr Canc Netw 2022;20:167-92.
6. Shinkai M, Imano M. The clinical effect of conversion surgery for advanced gastric cancer patients with peritoneal metastasis. J Gastrointest Oncol 2022;13:2169-77.
7. Yang Z, Lu S, Shi M, et al. Oncological outcomes of conversion therapy in gastric cancer patients with peritoneal metastasis: a large-scale retrospective cohort study. Gastric Cancer 2024;27:387-99.
8. Nakazawa N, Sohda M, Hosoi N, et al. Conversion Surgery After Chemotherapy Plus Nivolumab as the First-Line Treatment for Unresectable Advanced or Recurrent Gastric Cancer and a Biomarker Study Using the Gustave Roussy Immune Score: A Multicenter Study. Ann Surg Oncol 2024;31:9023-9.
9. Jin ZJ, Lu S, Shi M, et al. Perioperative systemic and prophylactic intraperitoneal chemotherapy for type 4/large type 3 gastric cancer: DRAGON-10. Future Oncol 2024;20:2833-8.
10. Shen Y, Yu S, Zhang Y, et al. The exploration of surgery and survival prediction in patients with peritoneal metastasis from gastric adenocarcinoma based on the SEER database. J Gastrointest Oncol 2024;15:597-611.
11. Liang S, Fang X, Jiang P, et al. Camrelizumab and apatinib combined with chemotherapy in perioperative effective therapy for advanced gastric carcinoma with peritoneal metastasis: a case report. J Gastrointest Oncol 2023;14:2658-67.
12. Wei YY, Cai JY, Wang LL, et al. Dynamic change in the peritoneal cancer index based on CT after chemotherapy in the overall survival prediction of gastric cancer patients with peritoneal metastasis. J Cancer Res Clin Oncol 2024;150:222.
13. Yang J, Su H, Chen T, et al. Development and validation of nomogram of peritoneal metastasis in gastric cancer based on simplified clinicopathological features and serum tumor markers. BMC Cancer 2023;23:64.
14. Xiong T, Wang Y, Zhu C. A risk model based on 10 ferroptosis regulators and markers established by LASSO-regularized linear Cox regression has a good prognostic value for ovarian cancer patients. Diagn Pathol 2024;19:4.
15. Chen L, Ge M, Mo S, et al. Construction of a New Ferroptosis-related Prognosis Model for Survival Prediction in Colorectal Cancer. Curr Med Chem 2024. [Epub ahead of print]. doi: 10.2174/0109298673296767240116215814.
16. Li D, Wang Y, Dong C, et al. CST1 inhibits ferroptosis and promotes gastric cancer metastasis by regulating GPX4 protein stability via OTUB1. Oncogene 2023;42:83-98.
17. Lin Z, Song J, Gao Y, et al. Hypoxia-induced HIF-1α/lncRNA-PMAN inhibits ferroptosis by promoting the cytoplasmic translocation of ELAVL1 in peritoneal dissemination from gastric cancer. Redox Biol 2022;52:102312.
18. Dixon SJ, Lemberg KM, Lamprecht MR, et al. Ferroptosis: an iron-dependent form of nonapoptotic cell death. Cell 2012;149:1060-72.
19. Li S, Shang X, Lou H, et al. Cascade Bilateral Regulation of Ferroptosis and Immune Activation Conducted by the Electron-Accepting-Inspired Glycopolymer-Based Nanoreactor. ACS Appl Mater Interfaces 2024;16:65809-21.
20. Sun J, Li J, Pantopoulos K, et al. The clustering status of detached gastric cancer cells inhibits anoikis-induced ferroptosis to promote metastatic colonization. Cancer Cell Int 2024;24:77.
21. Wang J, Jia Q, Jiang S, et al. POU6F1 promotes ferroptosis by increasing lncRNA-CASC2 transcription to regulate SOCS2/SLC7A11 signaling in gastric cancer. Cell Biol Toxicol 2024;40:3.

22. Ding L, Dang S, Sun M, et al. Quercetin induces ferroptosis in gastric cancer cells by targeting SLC1A5 and regulating the p-Camk2/p-DRP1 and NRF2/GPX4 Axes. Free Radic Biol Med 2024;213:150-63.
23. Wang H, Li C, Meng S, et al. The LINC01094/miR-545-3p/SLC7A11 Signaling Axis Promotes the Development of Gastric Cancer by Regulating Cell Growth and Ferroptosis. Biochem Genet 2024. doi: 10.1007/s10528-024-10959-3.
24. Wen W, Ertas YN, Erdem A, et al. Dysregulation of autophagy in gastric carcinoma: Pathways to tumor progression and resistance to therapy. Cancer Lett 2024;591:216857.
25. Li Y, Liu J, Wu S, et al. Ferroptosis: opening up potential targets for gastric cancer treatment. Mol Cell Biochem 2024;479:2863-74.
26. Chen X, Poetsch A. The Role of Cdo1 in Ferroptosis and Apoptosis in Cancer. Biomedicines 2024;12:918.
27. Qin J, Wang J, Bian Y, et al. D-A-D type based NIR fluorescence probe for monitoring the cysteine levels in pancreatic cancer cell during ferroptosis. Bioorg Chem 2024;146:107260.
28. Yang WS, SriRamaratnam R, Welsch ME, et al. Regulation of ferroptotic cancer cell death by GPX4. Cell 2014;156:317-31.
29. Feng H, Yu J, Xu Z, et al. SLC7A9 suppression increases chemosensitivity by inducing ferroptosis via the inhibition of cystine transport in gastric cancer. EBioMedicine 2024;109:105375.
30. Yang Z, Zou S, Zhang Y, et al. ACTL6A protects gastric cancer cells against ferroptosis through induction of glutathione synthesis. Nat Commun 2023;14:4193.
31. Ushiku H, Yamashita K, Ema A, et al. DNA diagnosis of peritoneal fluid cytology test by CDO1 promoter DNA hypermethylation in gastric cancer. Gastric Cancer 2017;20:784-92.
32. Nikhil K, Shah K. The significant others of aurora kinase a in cancer: combination is the key. Biomark Res 2024;12:109.
33. Polverino F, Mastrangelo A, Guarguaglini G. Contribution of AurkA/TPX2 Overexpression to Chromosomal Imbalances and Cancer. Cells 2024;13:1397.
34. Tham MS, Cottle DL, Zylberberg AK, et al. Deletion of Aurora kinase A prevents the development of polycystic kidney disease in mice. Nat Commun 2024;15:371.
35. Yang Y, Wang J, Wan J, et al. PTEN deficiency induces an extrahepatic cholangitis-cholangiocarcinoma continuum via aurora kinase A in mice. J Hepatol 2024;81:120-34.
36. Naso FD, Polverino F, Cilluffo D, et al. AurkA/TPX2 co-overexpression in nontransformed cells promotes genome instability through induction of chromosome mis-segregation and attenuation of the p53 signalling pathway. Biochim Biophys Acta Mol Basis Dis 2024;1870:167116.
37. Teli G, Maji L, Pal R, et al. Recent advancements in mechanistic research, therapeutic potential, and structure-activity relationships of aurora kinase inhibitors in cancer therapies. Bioorg Chem 2025;154:107976.
38. Lv C, Wang Y, Kong L, et al. Securinine inhibits carcinogenesis in gastric cancer by targeting AURKA-β-catenin/Akt/STAT3 and the cell cycle pathway. Phytomedicine 2024;130:155735.
39. Liu X, Li Z, Song Y, et al. AURKA induces EMT by regulating histone modification through Wnt/β-catenin and PI3K/Akt signaling pathway in gastric cancer. Oncotarget 2016;7:33152-64.
40. Chen H, Hu J, Xiong X, et al. AURKA inhibition induces Ewing's sarcoma apoptosis and ferroptosis through NPM1/YAP1 axis. Cell Death Dis 2024;15:99.
41. Mi Y, Chen L, Wang C, et al. AURKA knockdown inhibits esophageal squamous cell carcinoma progression through ferroptosis. Heliyon 2024;10:e28365.
42. Ye Y, Xu L, Zhang L, et al. Meningioma achieves malignancy and erastin-induced ferroptosis resistance through FOXM1-AURKA-NRF2 axis. Redox Biol 2024;72:103137.
43. Zuo Z, Zhou Z, Chang Y, et al. Ribonucleotide reductase M2 (RRM2): Regulation, function and targeting strategy in human cancer. Genes Dis 2022;11:218-33.
44. Zhang J, Wu Q, Xie Y, et al. Ribonucleotide reductase small subunit M2 promotes the proliferation of esophageal squamous cell carcinoma cells via HuR-mediated mRNA stabilization. Acta Pharm Sin B 2024;14:4329-44.
45. Das B, Jain N, Mallick B. piR-39980 mediates doxorubicin resistance in fibrosarcoma by regulating drug accumulation and DNA repair. Commun Biol 2021;4:1312.
46. Zhao Y, Zheng Y, Zhu Y, et al. M1 Macrophage-Derived Exosomes Loaded with Gemcitabine and Deferasirox against Chemoresistant Pancreatic Cancer. Pharmaceutics 2021;13:1493.
47. Zhong Z, Cao Y, Yang S, et al. Overexpression of RRM2 in gastric cancer cell promotes their invasiveness via AKT/NF-κB signaling pathway. Pharmazie 2016;71:280-4.
48. Abbasi M, Gupta V, Chitranshi N, et al. Molecular Mechanisms of Glaucoma Pathogenesis with Implications to Caveolin Adaptor Protein and Caveolin-Shp2 Axis. Aging Dis 2024;15:2051-68.

49. Timmins LR, Ortiz-Silva M, Joshi B, et al. Caveolin-1 promotes mitochondrial health and limits mitochondrial ROS through ROCK/AMPK regulation of basal mitophagic flux. FASEB J 2024;38:e23343.
50. Wang Z, Chen C, Shu J, et al. Single-cell N(6)-methyladenosine-related genes function within the tumor microenvironment to affect the prognosis and treatment sensitivity in patients with gastric cancer. Cancer Cell Int 2024;24:44.
51. Huang L, Xiong W, Cheng L, et al. Bioinformatics-based analysis of programmed cell death pathway and key prognostic genes in gastric cancer: Implications for the development of therapeutics. J Gene Med 2024;26:e3590.
52. Wang X, Lu B, Dai C, et al. Caveolin-1 Promotes Chemoresistance of Gastric Cancer Cells to Cisplatin by Activating WNT/β-Catenin Pathway. Front Oncol 2020;10:46.
53. Trono P, Ottavi F, Rosano' L. Novel insights into the role of Discoidin domain receptor 2 (DDR2) in cancer progression: a new avenue of therapeutic intervention. Matrix Biol 2024;125:31-9.
54. Akinjiyan FA, Ibitoye Z, Zhao P, et al. DDR2-regulated arginase activity in ovarian cancer-associated fibroblasts promotes collagen production and tumor progression. Oncogene 2024;43:189-201.
55. Wang YG, Xu L, Jia RR, et al. DDR2 Induces Gastric Cancer Cell Activities via Activating mTORC2 Signaling and Is Associated with Clinicopathological Characteristics of Gastric Cancer. Dig Dis Sci 2016;61:2272-83.
56. Ren L, Ren Q, Wang J, et al. miR-199a-3p promotes gastric cancer progression by promoting its stemness potential via DDR2 mediation. Cell Signal 2023;106:110636.
57. Go GW, Mani A. Low-density lipoprotein receptor (LDLR) family orchestrates cholesterol homeostasis. Yale J Biol Med 2012;85:19-28.
58. He L, Lu Y, Wang P, et al. Up-regulated expression of type II very low density lipoprotein receptor correlates with cancer metastasis and has a potential link to β-catenin in different cancers. BMC Cancer 2010;10:601.
59. Cai B, Huang Y, Liu D, et al. Identification of the ferroptosis-related gene signature and the associated regulation axis in lung cancer and rheumatoid arthritis. Genes Immun 2024;25:367-80.
60. Yang M, Zhan Y, Hou Z, et al. VLDLR disturbs quiescence of breast cancer stem cells in a ligand-independent function. Front Oncol 2022;12:887035.
61. Anari M, Karimkhanloo H, Nie S, et al. Lipidome profiling in advanced metabolic liver disease identifies phosphatidylserine synthase 1 as a regulator of hepatic lipoprotein metabolism. Cell Rep 2024;43:115007.
62. Marakasova E, Olivares P, Karnaukhova E, et al. Molecular chaperone RAP interacts with LRP1 in a dynamic bivalent mode and enhances folding of ligand-binding regions of other LDLR family receptors. J Biol Chem 2021;297:100842.
63. Pei L, Ouyang Z, Zhang H, et al. Thrombospondin 1 and Reelin act through Vldlr to regulate cardiac growth and repair. Basic Res Cardiol 2024;119:169-92.

Cite this article as: Sun X, Duan K, Shen X, Dong C, Zhou Y, Chen T, Li W, Li P, Wang P, Li D, Zhou J. Construction and validation of a nomogram model for predicting peritoneal metastasis in gastric cancer based on ferroptosis-relate genes and clinicopathological features. J Gastrointest Oncol 2025;16(1):264-280. doi: 10.21037/jgo-24-670